Cooperative dynamics in coupled noisy dynamical systems near a critical point: The dc superconducting quantum interference device as a case study

Antonio Palacios,[1,*] John Aven,[1,†] Patrick Longhini,[2,‡] Visarath In,[2,§] and Adi R. Bulsara[2,‖]
[1]*Nonlinear Dynamical Systems Group, Department of Mathematics & Statistics, San Diego State University, San Diego, California 92182, USA*
[2]*Space and Naval Warfare Systems Center, Code 2373, 53560 Hull Street, San Diego, California 92152-5001, USA*
(Received 5 May 2006; published 22 August 2006)

Dynamical systems that operate near the onset of coupling-induced oscillations can exhibit enhanced sensitivity to external perturbations under suitable operating parameters. This cooperative behavior and the attendant enhancement in the system response (quantified here via a signal-to-noise ratio at the fundamental of the coupling-induced oscillation frequency) are investigated in this work. As a prototype, we study an array of dc superconducting quantum interference device (SQUID) rings locally coupled, unidirectionally as well as bidirectionally, in a ring configuration; it is well known that each individual SQUID can be biased through a saddle-node bifurcation to oscillatory behavior. We show that biasing the array near the bifurcation point of coupling-induced oscillations can lead to a significant performance enhancement.

DOI: 10.1103/PhysRevE.74.021122 PACS number(s): 02.50.Ey, 85.25.Dq

I. INTRODUCTION

A generic feature of many nonlinear dynamical systems is high sensitivity to small external perturbations, especially when they are "tuned" near the onset of a bifurcation. This feature appears to be further enhanced when the system consists of a certain number of individual units tightly coupled in some fashion. These critical observations have led us to develop, through several theoretical and experimental works [1–4], the basic principles for a general mechanism for signal detection and amplification. We have focused our efforts, so far, on a large class of nonlinear devices whose behavior is governed by overdamped bistable dynamics of the form $\dot{x}=-\nabla U(x)$, where $U(x)$ is a potential energy function. In the absence of an external forcing term, the state point $x(t)$ will rapidly relax to one of two stable attractors, which correspond to the minima of $U(x)$. This behavior is, of course, universal in overdamped dynamical systems. When a certain number of units are coupled to one another, however, the coupling alone can lead to self-sustained oscillations, whose stability properties depend, among other things, on the coupling topology, i.e., which units are coupled with each other. More importantly, the coupling scheme can lead, under certain conditions, to significant performance enhancements in terms of sensitivity and signal output response, relative to background noise.

In this work, we investigate further the model-independent idea of coupling-induced oscillations for signal detection through the most sensitive of all magnetic sensors, the dc SQUID (superconducting quantum interference device) magnetometer [5]. Our goal is to study the dynamics of the coupling-induced oscillations, i.e., determine their existence criteria and stability properties, as well as the gain in sensitivity of an array of locally coupled dc SQUID rings. The work complements and extends the recent theoretical analysis of a network of globally coupled dc SQUID rings [6] to the more complicated case of local coupling. In addition, we lay out the requirements for future experimental work. The resulting array device could be used in a wide range of magnetic field detection applications that require high levels of sensitivity such as biomedical tracking of magnetic particles (e.g., MRI machines commonly used for diagnosing multiple sclerosis, brain tumors, and spinal infections), geological equipment (e.g., NASA explorers, and remote sensing equipment for oil and mineral prospecting), homeland defense (e.g., detection of explosives, and building security applications) [7–19], as well as specialized applications such as superconducting quantum interference filters (SQIFs) [20].

The paper is organized as follows. In Sec. II we present a brief background of basic SQUID theory; this section is intended for readers not familiar with the subject. In Sec. III we derive the model equations for an array of N dc SQUIDs unidirectionally coupled in a ring configuration. We perform a computational bifurcation analysis to determine the onset of oscillations, derive an analytic expression for their frequency via center manifold theory, and investigate the gains in signal output relative to background noise. In Sec. IV we extend the analysis to a bidirectionally coupled ring.

II. BACKGROUND: THE dc SQUID

The most sensitive of all magnetic sensors is the superconducting quantum interference device (SQUID). Developed about 1962, a SQUID consists of tiny loops of superconductors into which one incorporates Josephson junctions; these are made up of two superconductors separated by an insulating layer so thin that electrons can tunnel through. A

*Electronic address: palacios@euler.sdsu.edu
†Electronic address: chaotic_aven@yahoo.com
‡Electronic address: longhini@spawar.navy.mil
§Electronic address: visarath@spawar.navy.mil
‖Electronic address: bulsara@spawar.navy.mil

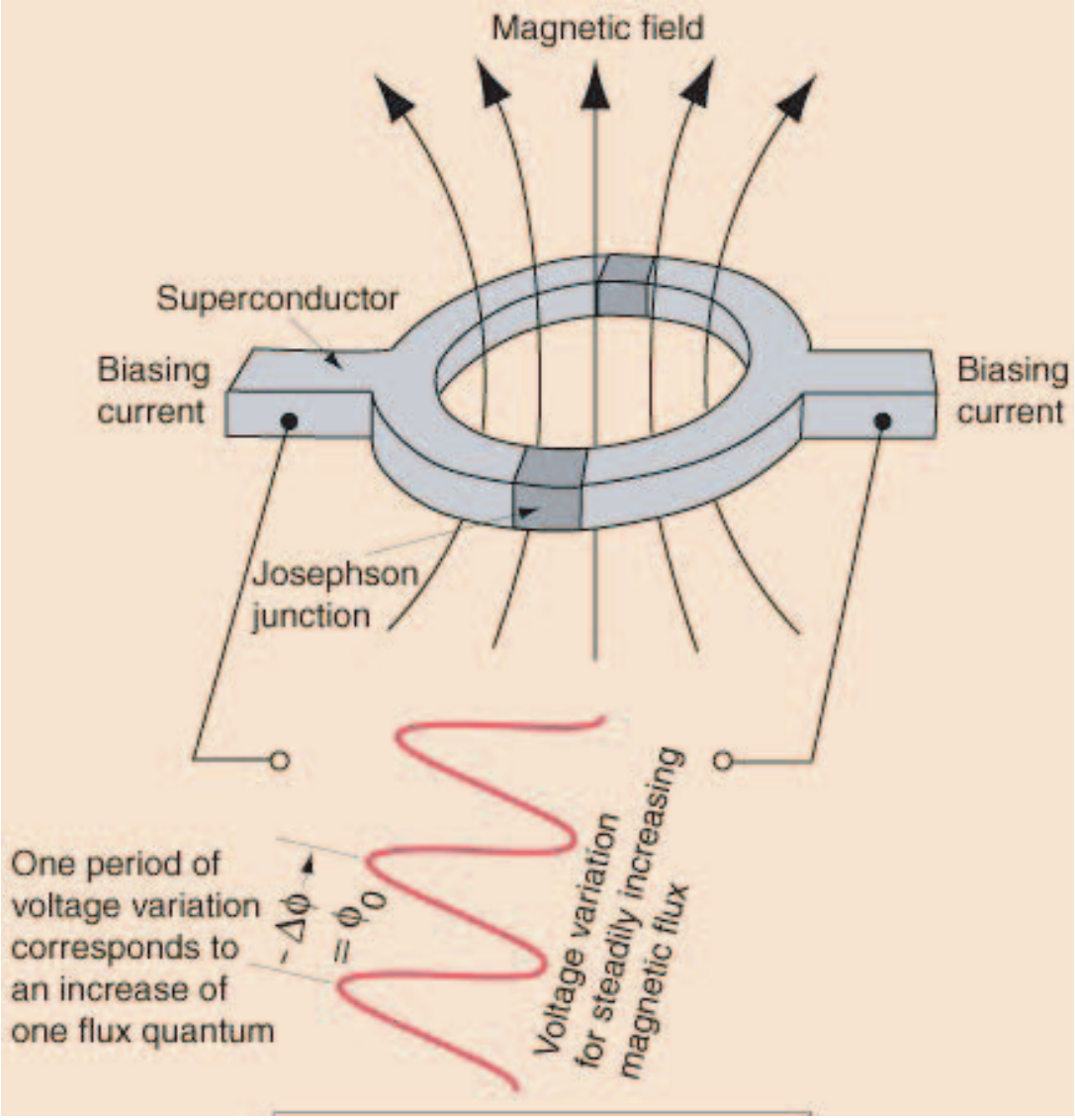

FIG. 1. (Color online) Schematic diagram of a dc SQUID magnetometer. Courtesy of www.phy-astr.gsu.edu.

radio frequency (rf) SQUID is made up of one Josephson junction mounted on a superconducting ring. An oscillating current is applied to an external circuit, whose voltage changes as an effect of the interaction between it and the ring. The magnetic flux is then measured. A direct current (dc) SQUID consists of two Josephson junctions employed in parallel so that electrons tunneling through the junctions demonstrate quantum interference, dependent upon the strength of the magnetic field within a loop. Today, SQUIDs boast of noise floors as low as $1-30$ fT/$\sqrt{\text{Hz}}$. We now provide an overview of the dynamics of a single dc SQUID, since this forms the "elemental unit" of the coupled array to be considered throughout this work. A more comprehensive description can be found in Ref. [5].

As already stated, the dc SQUID consists of two Josephson junctions inserted into a superconducting loop [5] (see Fig. 1); we assume, for convenience, that the insertion is symmetric. Conventionally, the voltage measured across the Josephson junctions is taken as the SQUID "output." It is, however, also convenient to take the circulating current I_s (experimentally measured via the associated "shielding flux") as the output variable of interest. Equation (7) and the discussion thereafter describe how to measure, numerically, the circulating current. Such a configuration setup was used, for example, in our earlier studies of the "stochastic resonance" effect in dc SQUIDs operating in the hysteretic regime [21,22]. However, much higher output signal strengths and response signal-to-noise ratios (SNRs) were discovered by using dc bias currents large enough to take the device beyond the hysteretic regime into the regime of oscillatory solutions. These higher input-output gains result from the rapid change of I_s with small changes in the (externally applied) magnetic flux Φ_e close to where the dynamics change from static to oscillatory.

In the presence of an external magnetic flux Φ_e, one obtains a loop flux consisting of the (geometrical) component Φ_e together with a contribution arising from the induced cir-

culating or shielding current I_s that tends to screen the applied flux:

$$\Phi = \Phi_e + LI_s, \tag{1}$$

L being the loop inductance. The Josephson currents in each arm of the "interferometer" are $I_0 \sin \delta_1$ and $I_0 \sin \delta_2$, with the junctions assumed to be identical with critical currents I_0, and with $\delta_{1,2}$ being the quantum phases. The wave function must remain single-valued around the SQUID loop, leading to the phase continuity condition

$$\delta_2 - \delta_1 = 2\pi n - 2\pi\Phi/\Phi_0, \tag{2}$$

n being an integer, and $\Phi_0 \equiv h/2e$ the flux quantum. Combining Eqs. (1) and (2) and setting $n=0$, we find for the circulating current I_s

$$\beta\frac{I_s}{I_0} = \delta_1 - \delta_2 - 2\pi\frac{\Phi_e}{\Phi_0}, \tag{3}$$

where $\beta \equiv 2\pi LI_0/\Phi_0$ is the nonlinearity parameter. In the absence of external magnetic flux signals we can use the resistively shunted Josephson junction (RSJ) model to write down equations for the currents in the two arms of the SQUID via a lumped circuit representation [5]; expressed via the Josephson relations $\dot{\delta}_i = 2eV_i/\hbar$ linking the voltage and the quantum phase difference across the junction i, these equations take the form

$$\tau\dot{\delta}_1 = \frac{I_b}{2} - I_s - I_0 \sin \delta_1, \quad \tau\dot{\delta}_2 = \frac{I_b}{2} + I_s - I_0 \sin \delta_2, \tag{4}$$

where $\tau \equiv \hbar/(2eR)$, R being the normal state resistance of the junctions. The dc bias current I_b is applied symmetrically to the loop. In experiments [21], the bias current and applied flux are, usually, externally controllable. This is a critical point since, as will become evident below, it permits us to manipulate the shape of the two-dimensional (2D) potential function that characterizes the SQUID dynamics and, thereby, the input-output transfer characteristic (TC) that governs the response [note that the solutions of Eq. (4) can be oscillatory, even in the absence of external inputs]. Rescaling time by τ/I_0, one can write the above in the form $\dot{\delta}_i = -\frac{\partial U}{\partial \delta_i}$ with the 2D potential function defined as

$$U(\delta_1, \delta_2) = -\cos \delta_1 - \cos \delta_2 - J(\delta_1 + \delta_2) + (2\beta)^{-1}(\delta_1 - \delta_2 - 2\pi\Phi_{ex})^2, \tag{5}$$

where we introduce the dimensionless bias current $J \equiv I_b/(2I_0)$ and normalized applied flux $\Phi_{ex} \equiv \Phi_e/\Phi_0$.

The SQUID's Josephson junctions are always in a zero-voltage state when the potential (5) has stable minima; it is readily apparent that the symmetry of the potential and the depth of the minima are controlled by the adjustable parameters J and Φ_{ex}. This configuration (including the problem of thermal activation out of the stable states of the potential) has been discussed in the literature [23]. After a brief transient, the phase angles $\delta_{1,2}$ achieve constant steady-state values and one obtains the conditions for the minima via $\dot{\delta}_{1,2} = 0$. This leads to the current equations

$$I_b = I_0(\sin \delta_1 + \sin \delta_2), \quad 2I_s = I_0(\sin \delta_2 - \sin \delta_1). \tag{6}$$

Of course, these equations may also be written down by applying Kirchoff's laws directly to the lumped circuit representation of the SQUID. Using the phase continuity relation, we are finally able to write down a transcendental equation for the circulating current I_s:

$$\frac{I_s}{I_0} = -\sin\left(\pi\Phi_{ex} + \frac{\beta I_s}{2I_0}\right) \times \cos\left[\sin^{-1}\left(J + \frac{I_s}{I_0}\right) + \pi\Phi_{ex} + \frac{\beta I_s}{2I_0}\right]. \tag{7}$$

Equation (7) may be solved numerically for the circulating current; the ensuing TC is periodic in the applied flux Φ_{ex} and possibly hysteretic, with the hysteresis loop width controlled by the bias current J. For $J=0$ one obtains hysteresis for any nonlinearity β; for $0 < J \leqslant 1$, hysteresis occurs over some range of β. It is most important to note that Eqs. (6) and therefore Eq. (7) are valid only when the potential has stable minima. In this regime, the externally applied bias current is matched by the sum of the junction supercurrents. When this balance is exceeded, a finite voltage V (corresponding to a normal loop current V/R) appears across the device. The maximum applied current (before the device enters its "voltage state") is clearly $2I_0$ in the absence of an applied external flux. However, in the presence of the external flux, one must compute the critical applied current at which the voltage state appears. In this regime, one obtains oscillatory solutions for the phases δ_i (modulo 2π) and the circulating current I_s, reminiscent of self-excited or relaxation oscillators that are encountered in systems with negative damping [24]. For the system at hand, this behavior may be traced to the description in terms of the two coupled first-order differential equations (4), together with a nonzero applied current J. In fact, it may be shown that, *only* in the zero-voltage regime (where the potential has stable minima), the SQUID dynamics (4) may be reduced to the 1D form, in terms of the normalized flux variable x:

$$\tau_s\dot{x} = -x - x_e - \frac{\beta}{2\pi} \sin \pi x \cos Z, \tag{8}$$

where we set $\tau_s = \frac{\beta\tau}{2I_0}$ and $Z = \pi x + \sin^{-1}\left(J + \frac{2\pi}{\beta}(x - x_e)\right)$. Equating the right hand side of Eq. (8) to zero and solving (numerically) for the x vs x_e TC yields a curve identical to that obtained from the transcendental form (7), after we express I_s in terms of x. Note that, in this regime, the potential (5) can readily be transformed into a single-variable potential $U(x)$, whose gradient yields (up to a multiplicative constant) the negative of the right hand side of Eq. (8); this, of course, is to be expected.

In this paper, we will be concerned, mainly, with the (voltage) state of stable periodic voltage oscillations, which occurs past a critical value J_c of the bias current. The oscillations are created via a global *saddle-node* bifurcation, in which the stable fixed (node) point collides with, and gets destroyed by, a saddle fixed point. To calculate the frequency of the spontaneous oscillations, a center manifold reduction of the nonlinear dynamics, represented by the coupled phase equations (4), near the singular point $J=J_c$ has been per-

formed [25]. The reduction effectively separates the slow dynamics in the vicinity of the center manifold from the fast dynamics of the complement space, which, after all, it eventually approaches that of the center manifold. More importantly, the reduction captures the frequency of the ensuing oscillations through the following analytical expression:

$$\Omega = \frac{1}{2\pi}\sqrt{F\alpha}, \tag{9}$$

where $F=(J-J_c)\cos\theta$, $\tan 2\theta=-\beta \sin\delta_0 \sin\Sigma_0$, (δ_0,Σ_0) is the equilibrium point (within the superconducting regime) of the nonlinear equations (4) expressed in the sum and difference variables $\delta=(\delta_1-\delta_2)/2$, $\Sigma=(\delta_1+\delta_2)/2$, and α is a parameter, introduced by the center manifold reduction, that depends on the equilibrium point (δ_0,Σ_0). It should be noted that the above expression (9) is most accurate very close to the critical point [25].

A. Coupled dc SQUID rings: A preamble

Coupled noisy dynamic systems have been extensively studied from the standpoint of spatiotemporal pattern formation [26] as well as the energetics associated with soliton propagation [27] in large arrays. The paper by Shiino [28] on a self-consistent mean-field description of coupled overdamped bistable elements remains one of the seminal works in this field, having spawned a plethora of papers on the dynamics of globally coupled noisy nonlinear dynamic elements. Synchronization in coupled systems has also remained a topic of considerable interest [29] with a significant number (too numerous to cite individually) of papers in the literature. During the 1990s, the advent of array enhanced stochastic resonance and its variations bred a rash of papers [30] dealing with the intriguing possibility of significantly enhanced system response (characterized by output SNRs or information-theoretic measures for nonsinusoidal input signals).

Some preliminary results on globally coupled dc SQUIDs in the presence of noise were first published by Inchiosa and Bulsara [31]. They presented a very careful discussion on the potential enhancement of the SNR response to a time-sinusoidal subthreshold target signal when one summed the response from each SQUID in an uncoupled network, pointing out that the summing circuit would, in fact, introduce a *de facto* coupling of the SQUIDs. The effects of correlated and uncorrelated noise were also examined, and precise bounds on the amount of enhancement laid out. Among their results was the fact that very strong coupling could eliminate any SNR enhancement and an optimal value of the coupling coefficient existed at which the maximal SNR enhancement occurred.

In Ref. [6] we considered a globally coupled network of dc SQUID rings. The onset of the running solutions was analyzed for the deterministic case and the average screening current computed from a Fokker-Planck description of the system in the presence of (small) noise sources in each ring. In addition, the effects of introducing a "probe" signal (taken as a deterministic sinusoid) in the flux or bias current variables were analyzed. In practice, this signal could be used to determine the underlying frequency of the SQUID oscillations by sweeping its frequency and seeking the resonance when it matches the internal oscillation frequency. At this resonance, one observes a significant depression in the noise floor of the response power spectral density (psd) at all frequencies with the most pronounced effect occurring at the fundamental. This effect, which has also been quantified in a single dc SQUID [2], can be exploited in SQUID networks to detect a very weak time-periodic external signal, by sweeping the internal oscillation frequency (through an adjustment of, say, the bias currents) until it resonates with the target signal frequency.

In recent work, we have considered the idea of *unidirectional* coupling in arrays (possibly overdamped) of nonlinear dynamic elements with cyclic boundary conditions [3,32,33]. The results show that coupling $N>2$ such elements can lead to oscillatory behavior past a critical point characterized by a critical value of the coupling constant. The "oscillations" in this case correspond to transitions across the potential energy barriers of the state point of each element with a transition rate (oscillation frequency) that can be exactly computed for the deterministic case and exhibits a characteristic square-root scaling with the "bifurcation distance" (the separation of the coupling constant from its critical value). These oscillations occur even in the absence of any external forcing, as long as at least one of the initial states of the elements is different from the rest; in practice, one always must provide power to assorted circuit elements (most notably the coupling circuits) so that no fundamental laws are violated. The effects of very small target signals (dc [3] and time-sinusoidal [32]) on the oscillation characteristics can be exploited to detect and quantify the unknown target signals. These phenomena are now being exploited in a new class of room temperature magnetic [4] and electric field [33] detectors. The effects of noise in these systems are, only recently, becoming clear, with significant amplification (via an array enhanced coherence resonance effect) possible with increasing N [34], as well as the generation of spatiotemporal patterns together with solitonlike disturbances and the (noise-induced) creation or annihilation of domain walls, in large arrays [35].

dc SQUIDs, coupled in a topolgy that bears some similarities to the unidirectional coupling discussed in the preceding paragraph, are being developed as ultrasensitive, very wide-band signal filters. These so-called superconducting quantum interference filters (SQIFs) [20] are expected to find significant applications in applications like biomedical imaging, magnetic signal detection in specialized applications, and antennas. However, the dynamics (together with the effects of background noise) of these (locally coupled) arrays have not been worked out in great detail. In what follows, we take the first steps towards this goal, considering cyclically coupled dc SQUID rings with local (unidirectional as well as bidirectional) interelement coupling.

III. UNIDIRECTIONALLY COUPLED dc-SQUID RINGS

A. Model equations

We consider an array of N dc SQUID rings arranged in a ring configuration, unidirectionally coupled, so that the flux

Φ_k in each individual SQUID k depends on one of its nearest neighbors, that is

$$\Phi_k = \Phi_e + L_k I_k + M I_{k+1}, \quad k = 1, \ldots, N, I_{N+1} = I_1 \tag{10}$$

where M is the coupling strength. This configuration is similar to the one we used in the study of coupled-core fluxgate magnetometers [3], except that now the internal dynamics of each individual unit involves the phase differences of the Josephson junctions instead of a macroscopic magnetic flux variable (in the coupled-core fluxgate magnetometer). The case of bidirectional coupling will be discussed in Sec. IV. Then, this paper is expected to complement and extend our previous work [6]. Substituting Φ_k into Eq. (2) leads to the following system of differential equations for the array dynamics:

$$\frac{\tau_k}{I_{0k}} \dot{\delta}_{kj} = J_k + (-1)^j \frac{I_k}{I_{0k}} - \sin(\delta_{kj}),$$

$$\beta_k \frac{I_k}{I_{0k}} = \delta_{k1} - \delta_{k2} - 2\pi x_e - 2\pi\lambda I_{k+1}, \tag{11}$$

where $k=1,\ldots,N$ mod N, $j=1,2$, $\beta_k = 2\pi L_k I_{0k}/\Phi_0$, and λ is the coupling strength normalized by the flux quantum, i.e., $\lambda = M/\Phi_0$. L_k is the loop inductance of the kth element, I_k is its screening current (normalized to the critical current I_{0k}), and J_k is the loop bias current. The implications of this coupling scheme, from an experimental point of view, will be discussed in more detail in the final section of this manuscript.

To solve for I_k we set up an iterative method as follows. We write the second equation in Eq. (11) in matrix form $(A+B)I=\Delta$, where

$$A = \begin{bmatrix} \frac{\beta_1}{I_{01}} & 0 & 0 & \ldots & 0 \\ 0 & \frac{\beta_2}{I_{02}} & 0 & \ldots & 0 \\ \vdots & & & \ddots & \vdots \\ 0 & 0 & 0 & \ldots & \frac{\beta_N}{I_{0N}} \end{bmatrix},$$

$$B = 2\pi\lambda \begin{bmatrix} 0 & 1 & 0 & \ldots & 0 \\ 0 & 0 & 1 & \ldots & 0 \\ \vdots & & & \ddots & \vdots \\ 1 & 0 & 0 & \ldots & 0 \end{bmatrix},$$

$$I = \begin{bmatrix} I_1 \\ I_2 \\ \vdots \\ I_N \end{bmatrix},$$

$$\Delta = \begin{bmatrix} \delta_{11} - \delta_{12} - 2\pi x_e \\ \delta_{21} - \delta_{22} - 2\pi x_e \\ \vdots \\ \delta_{N1} - \delta_{N2} - 2\pi x_e \end{bmatrix}.$$

Direct iterations of $AI^{m+1} = \Delta - BI^m$ yield

$$I = C\Delta, \quad C = (I_d + A^{-1}B)^{-1}A^{-1}, \tag{12}$$

where I_d is the identity matrix of dimension N and C is an $N \times N$ matrix with the following structure:

$$C = \frac{1}{\left(\frac{\beta_1}{I_{01}}\frac{\beta_2}{I_{02}}\cdots\frac{\beta_N}{I_{0N}}\right) - \varepsilon^N} \left[\begin{array}{c|c|c|c} \frac{\beta_2}{I_{02}}\frac{\beta_3}{I_{03}}\cdots\frac{\beta_N}{I_{0N}} & -\frac{\beta_3}{I_{03}}\frac{\beta_4}{I_{04}}\cdots\frac{\beta_N}{I_{0N}}\varepsilon & \frac{\beta_4}{I_{04}}\frac{\beta_5}{I_{05}}\cdots\frac{\beta_N}{I_{0N}}\varepsilon^2 & \cdots \quad (-\varepsilon)^{N-1} \\ (-\varepsilon)^{N-1} & \frac{\beta_1}{I_{01}}\frac{\beta_3}{I_{03}}\cdots\frac{\beta_N}{I_{0N}} & -\frac{\beta_1}{I_{01}}\frac{\beta_4}{I_{04}}\cdots\frac{\beta_N}{I_{0N}}\varepsilon & \cdots \quad \frac{\beta_1}{I_{01}} \\ \vdots & & & \ddots \quad \vdots \\ -\frac{\beta_2}{I_{02}}\frac{\beta_3}{I_{03}}\cdots\frac{\beta_{N-1}}{I_{0,N-1}}\varepsilon & \frac{\beta_{N-1}}{I_{0,N-1}}\varepsilon^2 & (-\varepsilon)^{N-1} & \cdots \quad \frac{\beta_1}{I_{01}}\frac{\beta_2}{I_{02}}\cdots\frac{\beta_{N-1}}{I_{0,N-1}} \end{array}\right], \tag{13}$$

in which $\varepsilon = 2\pi\lambda$. We observe that the local coupling scheme (10) facilitates the calculation of a closed form solution for C, as opposed to the case of global coupling where such solution does not exist [6]. Furthermore, the structure of C indicates that the phase dynamics of each individual SQUID depend on the phases of every other SQUID in the ring. Interestingly, the phases become globally coupled to one another even though the circulating currents are only locally coupled. We now write the phase dynamics of the k SQUID using the closed form for C as follows:

$$\frac{\tau_k}{I_{0k}} \dot{\delta}_{kj} = J_k + (-1)^j \sum_{i=1}^{N} \frac{C_{ki}}{I_{0k}} (\delta_{i1} - \delta_{i2} - 2\pi x_e) - \sin(\delta_{kj}), \tag{14}$$

where $k=1,\ldots,N$ mod N and $j=1,2$.

B. Onset of oscillations: Bifurcation analysis

In what follows we consider SQUIDs with identical junctions, i.e., the same critical current $I_{0k}=I_0$, the same normal

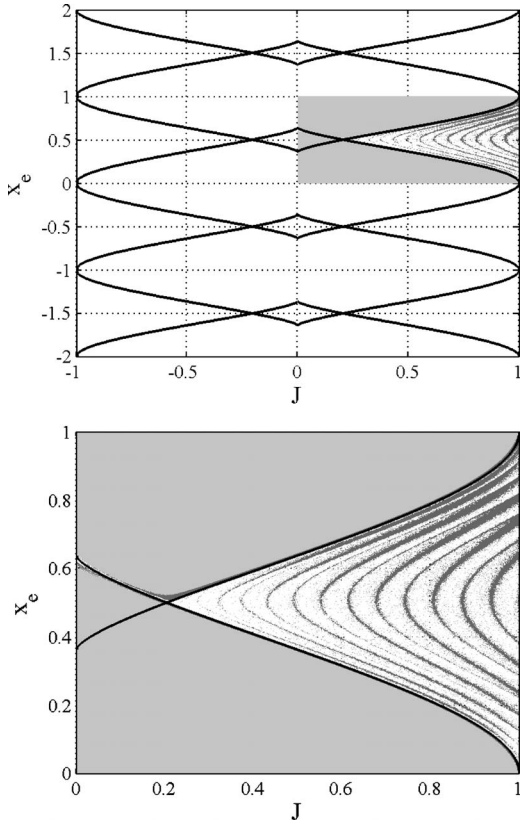

FIG. 2. (Top) Two-parameter bifurcation diagram describing the boundary of existence of steady-state solutions (SS) and of periodic solutions (RS) for a ring of three SQUIDs coupled unidirectionally. (Bottom) In the gray-shaded area of the plot, periodic solutions exist only inside the triangular region. In that triangular region, black (white) bands denote trajectories with long-term (short-term) transient behavior. Outside of the triangular region trajectories converge to a steady-state solution. Similar behavior is observed in equivalent areas of the two-parameter space shown in the top of this figure. Parameters are $\lambda=0.01$, $\beta_k=0.8$. Flux oscillations within the RS regime are completely synchronized with one another, i.e., the same amplitude and the same phase.

resistance $R_k=R_0$, and the same bias current J_k. All analytic calculations are carried out assuming different values of β, which may arise in experiments due to differences in loop inductances L_k, but most computer simulations are performed with identical β values. Under these conditions, the coupled SQUID system generically exhibits two patterns of behavior: a steady-state solution (SS), in which the long-term dynamics of each individual SQUID settles into an equilibrium state; and a running solution (RS), in which the flux in each SQUID oscillates, periodically, as a function of time. The oscillations emerge via a saddle-node bifurcation, just as in the case of a single SQUID. Figure 2 is a two-parameter bifurcation diagram which depicts, in parameter space (J,Φ_e), the basin boundary of existence of both types of solutions, steady states and periodic oscillations, for a ring of $N=3$ SQUIDs coupled unidirectionally. The symmetries in the diagram are a direct consequence of reflectional symmetries in the model (14) and of the periodicity of the phase variables. Running solutions exist only inside triangular regions, one of which is represented in the shaded area. Within

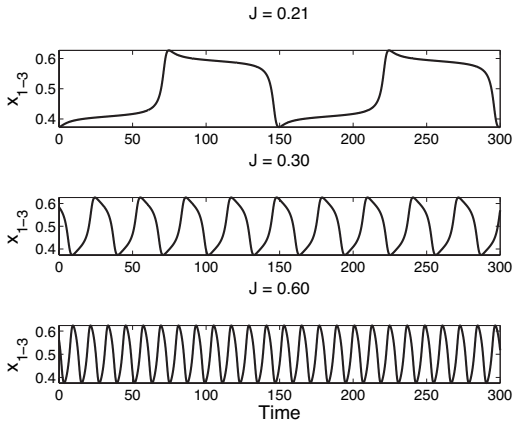

FIG. 3. Wave forms of flux oscillations in a ring of $N=3$ SQUIDs coupled unidirectionally with various values of bias current J. In each case, flux oscillations are completely synchronized with one another, i.e., the same amplitude and the same phase. Close to their onset of existence (tip of triangular region in Fig. 2), the wave forms show a relaxationlike structure. As the bias current increases, the wave forms gradually approach a more sinusoidal shape. Parameters are $x_e=0.5$, $\beta_k=0.8$, and $\lambda=0.01$.

that triangular region, black bands correspond to parameter values where typical trajectories, with random initial conditions, show long-transient behavior. Likewise, white bands denote trajectories with short-transient behavior. On the boundary lines that extend, symmetrically, to the left of the tip of the triangular region, there are no oscillations, only long transients which eventually settle into a (constant) steady-state solution. The structure of this basin boundary of attraction is similar to those of the globally coupled networks of SQUIDs considered by Acebron *et al.* [6]. The actual onset of oscillations, in terms of the critical values for the bias current J and the external flux x_e, can also be calculated analytically following the procedure described in Ref. [6],

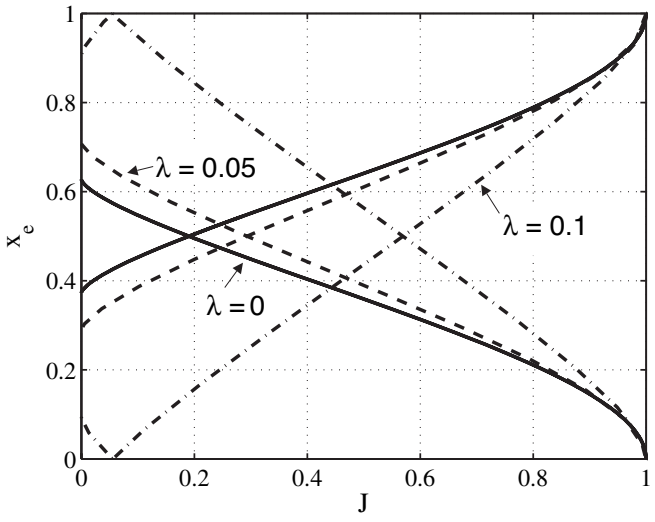

FIG. 4. Two-parameter continuation of running solutions and steady states in a three-SQUID ring system, unidirectionally coupled with various values of coupling strength λ. Increasing the coupling strength has the effect of shifting the critical bias current J_c horizontally. Parameters are $\beta_k=0.8$.

except that the matrix C of Eq. (13) must now be used. Similar basins of attraction are found for larger rings, including those with odd and even values of N.

Within the RS regime of Fig. 2, all flux oscillations are completely synchronized with one other, i.e., they all exhibit the same amplitude and the same phase. The wave form changes, however, with different values of the bias current J. For bias current values close to the onset of the oscillations, in particular, the flux variations have a typical relaxation oscillation shape. But as J increases, the wave form gradually approaches a more sinusoidal shape, as shown in Fig. 3. Observe also that the frequency of the oscillations increases as J increases. Each individual flux variable was calculated using the formula $x_k=(\delta_{k1}-\delta_{k2})/2\pi$. Increasing the coupling strength in the ring does not destroy, in general, the structure of the basin boundaries of attractions of the running solutions and of the steady states; the main effect is, however, to shift, horizontally, the onset point $(J_c, x_e=0.5)$ towards the right, as is shown in Fig. 4. There is, however, a maximum value of coupling strength λ_{max}, beyond which all oscillations cease to exist. To investigate what that maximum value of coupling strength is, we now fix the external flux x_e and track the J component of the boundary of the triangular region that bounds the running solution (Fig. 4), as a function of coupling strength. The resulting bifurcation diagram is shown in Fig. 5 for three fixed values of external flux, $x_e=0.05$, $x_e=0.3$, and $x_e=0.5$. The diagram shows that, for any particular fixed value of x_e, oscillations occur for values of (λ, J) that lie above the curve associated with that same value of x_e. More importantly, the diagram confirms that, indeed, there is a maximum coupling strength (value of λ farthest to the right along the bifurcation curves) beyond which all oscillations disappear and the system quickly settles into a steady state. However, for values of λ significantly larger than λ_{max} the system exhibits several complex transitions, via Hopf bifurcations, to additional dynamic states such as quasiperiodic oscillations with various frequencies of oscillation. The region of existence and stability of these new dynamic states is very interesting indeed but we refer their analysis for future work.

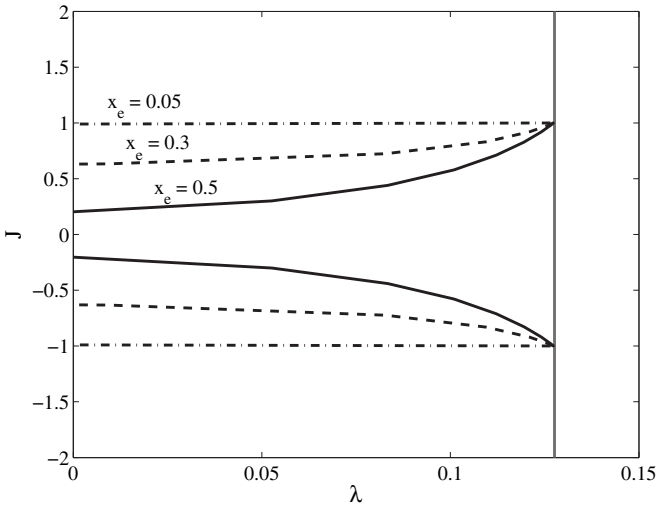

FIG. 5. Two-parameter continuation, in terms of bias current and coupling strength, of running solutions in a three-SQUID ring system, unidirectionally coupled. For a fixed value of x_e, oscillations occur for values of (λ, J) that lie above the curve with that same value of x_e. The maximum coupling strength that permits oscillations is the value of λ farthest to the right (vertical line) along the bifurcation curves. Parameters are $\beta_k=0.8$.

In order to find an analytical expression for λ_{max}, we first write the matrix C in powers of λ, as is shown below:

$$C=\begin{bmatrix} \frac{1}{\beta_1}I_0 & -\frac{1}{\beta_1\beta_2}I_0^2\varepsilon & 0 & \cdots & 0 \\ 0 & \frac{1}{\beta_2}I_0 & -\frac{1}{\beta_2\beta_3}I_0^2\varepsilon & \cdots & 0 \\ \vdots & & & \ddots & \vdots \\ -\frac{1}{\beta_1\beta_N}I_0^2\varepsilon & 0 & 0 & \cdots & \frac{1}{\beta_N}I_0 \end{bmatrix}+O(\lambda^2).$$

Then we rescale time by τ/I_0, so that the phase dynamics takes the new form

$$\dot{\delta}_{kj}=J+\frac{(-1)^j}{\beta_k}\left(\delta_{k1}-\delta_{k2}-2\pi x_e-2\pi\lambda\frac{I_0}{\beta_{k+1}}(\delta_{k+1,1}-\delta_{k+1,2}-2\pi x_e)\right)-\sin(\delta_{kj})+O(\lambda^2), \quad (15)$$

where $k=1,\ldots,N$ mod N and $j=1,2$. Observe that now the phase dynamics of each individual SQUID k depends only on that of its nearest neighbor $k+1$, in a manner that is consistent with the unidirectional coupling scheme. We will also use this new form of the phase dynamics later when we calculate an analytic expression for the frequency response of the oscillations. Returning to the case of λ_{max}, we set $x_e=0$ in Eq. (15) for simplicity, since λ_{max} is the same for any value of x_e and assume all SQUIDs to be identical, i.e., $\beta_k=\beta$. At λ_{max}, all phases variables are constant, so the system

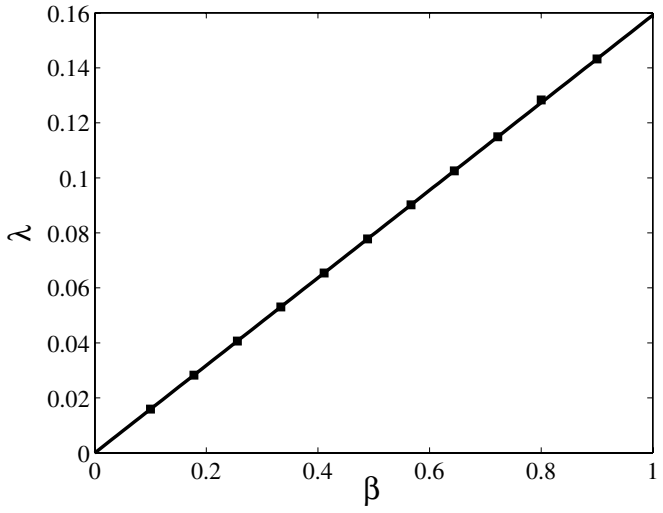

FIG. 6. Comparison between analytical (solid line) and numerical (dot markers) calculations of the maximum coupling strength that can yield flux oscillations in an array of three SQUIDs, unidirectionally coupled in a ring configuration. Parameters are $x_e=0.5$, $J=0.5$, and $\beta_k=0.8$.

is in an equilibrium, i.e., $\dot{\delta}_{k1}=\dot{\delta}_{k2}=0$, which leads to the following equation:

$$\frac{2}{\beta}\left(\delta_{k1}-\delta_{k2}-2\pi x_e-\frac{2\pi\lambda}{\beta}(\delta_{k+1,1}-\delta_{k+1,2}-2\pi x_e)\right)+\sin\delta_{k1}-\sin\delta_{k2}=0. \tag{16}$$

Furthermore, as $\lambda\rightarrow\lambda_{max}^{-}$ the coupled system quickly converges to a complete synchronization state in which all phase variables are in-phase with one another, i.e., $\delta_{k1}=\delta_{k+1,1}$, $\delta_{k2}=\delta_{k+1,2}$, and $\delta_{k1}=\delta_{k2}$. Substituting these relations into Eq. (16) yields

$$\frac{2}{\beta}\left(-2\pi x_e+\frac{(2\pi)^2 x_e\lambda}{\beta}\right)=0.$$

Simplifying this last equation shows that λ is independent of x_e, while solving for λ we obtain

$$\lambda_{max}^{u}=\frac{\beta}{2\pi}, \tag{17}$$

where the superscript u indicates that the ring is unidirectionally coupled. We note that this result holds for arbitrary N. From a physical point of view, the fact that λ_{max} is independent of x_e can be attributed to the robustness of the coupling-induced oscillations, i.e., a perturbation of the system by an external flux does not change the limit-point bifurcation of the critical coupling where oscillations commence (or stop). In Fig. 6 we compare the analytical value of λ_{max} produced by Eq. (17) against numerical calculations. Both results, analytical and numerical, show the linear dependence of the coupling strength on the parameter β, and are in very good agreement with one another.

C. Frequency dependence

To calculate the actual frequency of the ensuing oscillations, we consider the dynamics of the ring system near the bifurcation point $J=J_c$, which is now assumed to be identical for all SQUIDs. In order to facilitate further calculations, we rewrite Eq. (15) in terms of the difference and sum variables $\delta_k=(\delta_{k1}-\delta_{k2})/2$ and $\Sigma_k=(\delta_{k1}+\delta_{k2})/2$, leading to

$$\dot{\delta}_k=-\frac{1}{\beta_k}(2\delta_k-2\pi x_e)+2\pi\lambda\frac{I_0}{\beta_k\beta_{k+1}}(2\delta_{k+1}-2\pi x_e)-\cos\Sigma_k\sin\delta_k$$

$$\dot{\Sigma}_k=J-\cos\delta_k\sin\Sigma_k. \tag{18}$$

Let $(\delta_{k0},\Sigma_{k0})$ denote the fixed point of each individual, uncoupled, SQUID. Also let $x_k=\delta_k-\delta_{k0}$, $y_k=\Sigma_k-\Sigma_{k0}$. A Taylor series expansion of Eq. (18) about $J-J_c$, up to third order, yields

$$\dot{x}_k=-\left(\frac{2}{\beta_k}+A_k\right)x_k+B_k y_k+\frac{\varepsilon I_0}{\beta_k\beta_{k+1}}(2\delta_{k+1,0}-2\pi x_e)+\frac{2\varepsilon I_0}{\beta_k\beta_{k+1}}x_{k+1}+C_k x_k^2+2D_k x_k y_k+C_k y_k^2,$$

$$\dot{y}_k=(J-J_c)-A_k y_k+B_k x_k+D_k y_k^2+2C_k x_k y_k+D_k x_k^2,$$

$$\dot{J}=0,$$

$$\dot{\lambda}=0, \tag{19}$$

where $A_k=\cos\Sigma_{k0}\cos\delta_{k0}$, $B_k=\sin\Sigma_{k0}\sin\delta_{k0}$, $C_k=(1/2)\cos\Sigma_{k0}\sin\delta_{k0}$, and $D_k=(1/2)\sin\Sigma_{k0}\cos\delta_{k0}$.

The basic strategy is, now, to determine the frequency of the ensuing oscillations from a reduction of Eq. (19) to its center manifold. We prepare Eq. (19) for the center manifold reduction by introducing the following change of coordinates:

$$\begin{bmatrix}u_1\\v_1\\\vdots\\u_N\\v_N\end{bmatrix}=S\begin{bmatrix}x_1\\y_1\\\\x_N\\y_N\end{bmatrix},$$

$$S=\begin{bmatrix}\cos\theta_1 & -\sin\theta_1 & \cdots & 0 & 0\\ \sin\theta_1 & \cos\theta_1 & \cdots & 0 & 0\\ \vdots & & \ddots & & \vdots\\ 0 & 0 & \cdots & \cos\theta_N & -\sin\theta_N\\ 0 & 0 & \cdots & \sin\theta_N & \cos\theta_N\end{bmatrix}. \tag{20}$$

The variables θ_k in the diagonalization matrix S are obtained through the relation $\tan 2\theta_k=-\beta_k\sin\Sigma_{k0}\cos\delta_{k0}$. Now direct calculations show that the eigenvalues of the linear part of Eq. (19) are

$$\Psi_1 = 0,$$

$$\Psi_{-1} = -\frac{2}{\beta_1} - 2A_1,$$

$$\Psi_{\pm k} = -\frac{1}{\beta_k} - 2A_k \pm \frac{1}{\beta_k}\frac{1}{\cos 2\theta_k}, \quad k = 2, \ldots, N.$$

Then, when we use the change of coordinates (20), the first two sets of equations in Eq. (19) become

$$\begin{bmatrix} \dot{u}_1 \\ \dot{v}_1 \\ \vdots \\ \dot{u}_N \\ \dot{v}_N \end{bmatrix} = \begin{bmatrix} 0 & 0 & 0 & 0 & \ldots & 0 & 0 \\ 0 & -\frac{2}{\beta_1} - 2A_1 & 0 & 0 & \ldots & 0 & 0 \\ \vdots & & & & \ddots & & \vdots \\ 0 & 0 & 0 & 0 & \ldots & \Psi_{-N} & 0 \\ 0 & 0 & 0 & 0 & \ldots & 0 & \Psi_N \end{bmatrix} \begin{bmatrix} u_1 \\ v_1 \\ \vdots \\ u_N \\ v_N \end{bmatrix}$$

$$+ S \begin{bmatrix} D_1 y_1^2 + 2C_1 x_1 y_1 + D_1 x_1^2 \\ 2\varepsilon I_0 x_2 + C_1 x_1^2 + 2D_1 x_1 y_1 + C_1 x_1^2 \\ \vdots \\ D_N y_N^2 + 2C_N x_N y_N + D_N x_N^2 \\ 2\varepsilon I_0 x_1 + C_N x_N^2 + 2D_N x_N y_N + C_N x_N^2 \end{bmatrix}. \quad (21)$$

Numerical calculations show that the eigenvalues of Eq. (21) are either negative or zero, thus all trajectories will exponentially relax to the center eigenspace $u_1=0$. It follows, from center manifold theory, that the stability of the equilibrium points $(\delta_{k0}, \Sigma_{k0})$ near $J=J_c$ can be determined by a one-parameter family of first-order differential equations described by the u_1 and ε variables. To compute the center manifold, we first assume the dynamics has already relaxed to the center eigenspace $u_1=0$ so that $\dot{u}_2=0, \ldots, \dot{u}_N=0$ and $\dot{v}_1=0, \ldots, \dot{v}_N=0$. Then we solve the resulting algebraic equations for $u_i=h_i(u_1,\varepsilon)$, $i=2,\ldots,N$ and $v_j=h_{j+N}(u_1,\varepsilon)$, $j=1,\ldots,N$. Once these algebraic equations have been solved, the evolution of u_1 on the center manifold becomes

$$\dot{u}_1 = (J - J_c)\cos\theta_1 - \frac{\varepsilon}{\beta_1\beta_2}(2\delta_{20} - 2\pi x_e)\sin\theta_1 + \alpha u_1^2 + 2\gamma\frac{\varepsilon^2}{\beta_1}u_1 + O[(J-J_c)^3], \quad (22)$$

where

$$\eta_2 = (2/\Psi_2)\cos\theta_2 \sin\theta_1,$$

$$\xi_2 = (2/\Psi_{-2})\sin\theta_2 \sin\theta_1,$$

$$\alpha = \cos\theta_1(D_1 - C_1 \sin 2\theta_1) - \sin\theta_1(C_1 - D_1 \sin 2\theta_1),$$

$$\gamma = (1/\beta_2)(\xi_2 \cos\theta_2 \sin\theta_1 - \eta_2 \cos\theta_2 \sin\theta_1).$$

Effectively, the transformation (20) and the center manifold reduction allows us to separate the *slow* dynamics on the eigenspace $u_1=0$ from the *fast* dynamics on the space $(v_1, u_2, v_2, \ldots, u_N, v_N)$, which eventually decays to zero. Moreover, integrating Eq. (22) we get

$$u_1(t) = \sqrt{\frac{F_u}{\alpha} - \frac{\gamma^2\varepsilon^4}{\alpha^2}}\tan(\sqrt{F_u\alpha - \gamma^2\varepsilon^4}\,t) - \frac{\gamma\varepsilon^2}{\alpha}, \quad (23)$$

where $F_u=(J-J_c)\cos\theta_1 - [\varepsilon/(\beta_1\beta_2)](2\delta_{20} - 2\pi x_e)\sin\theta_1$. It follows that the frequency of the oscillations of the coupled-SQUID system (15) is given by

$$\omega_u = \frac{1}{2\pi}\sqrt{F_u\alpha - \gamma^2\varepsilon^4}. \quad (24)$$

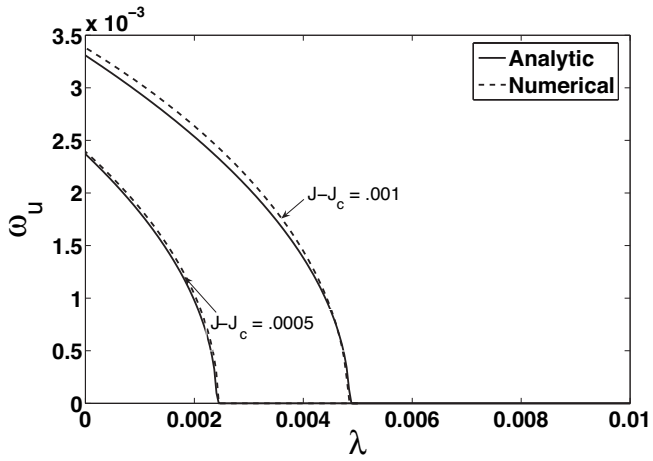

FIG. 7. Frequency response of a three-SQUID, unidirectionally, coupled ring system as a function of coupling strength. Parameters are $x_e=0.5$ and $\beta_k=0.8$.

Observe that Eq. (24) has essentially the same structure as that of the frequency response for the all-to-all network configuration studied by Acebron *et al.* [6]. This similarity results from the fact that the ring dynamics on the center manifold, as is described by Eq. (23), has the same form as that of the all-to-all network. However, a significant difference between these two cases (all-to-all and directed rings) is in the term F, which now depends only on the phase dynamics of one single SQUID. Consequently, the frequency response of our directed-ring configuration is independent of the number of SQUIDs in the ring. This result is in direct contrast to the frequency response of the all-to-all network configuration of Ref. [6], in which the mean-field-type coupling leads to a frequency dependence on the number of SQUIDs. Observe also that when the SQUIDs are decoupled, i.e., when $\lambda=0$, then $\varepsilon=0$ and the frequency response ω_u in Eq. (24) reduces to the frequency response Ω of a single SQUID element given by Eq. (9), as expected. Figure 7 shows now a comparison of the frequency response of a three-SQUID ring system obtained numerically from simulations of the model equations (14) and analytically through Eq. (24). Both the analytical frequency response and the computational result show a characteristic dependence on the coupling strength λ that follows a square-root scaling law. More importantly, the

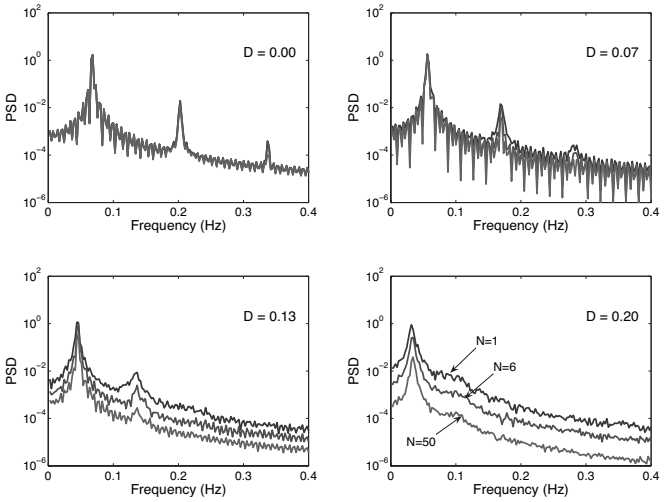

FIG. 8. Average PSD response of a *N*-SQUID ring system, unidirectionally coupled, to various values of noise intensity. Parameters are $J=0.5$, $x_e=0.5$, $\beta_k=0.8$, $\lambda=0.01$. Observe that in each individual panel the noise floor decreases as the number of SQUIDs increases. In all three cases, noise floor rises, however, as the noise intensity increases.

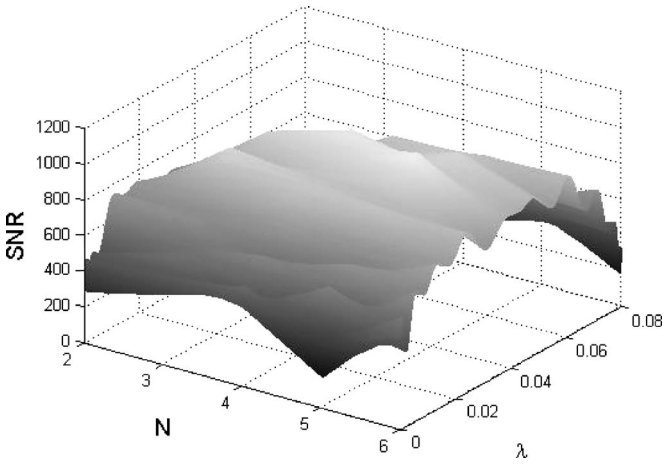

FIG. 9. Average signal-to-noise-ratio response of a *N*-SQUID ring system, unidirectionally coupled, as a multifunction of coupling strength λ and of the number of SQUIDs *N*. Parameters are $J=0.8$, $x_e=0.5$, $\beta_k=0.8$, $D=0.5$.

analytical frequency response is in good agreement, especially for small values of $J-J_c$, with numerical computations. Furthermore, we also note that coupling-induced oscillations only exist in the supercritical regime, i.e., past the critical coupling strength, regardless of whether *N* is even or odd.

D. Effects of noise and of varying the ring size

We now investigate the response of a unidirectionally coupled *N*-SQUID ring system to thermal noise through a Langevin version of the deterministic model equations (15) as follows:

$$\dot{\delta}_{kj} = J + \frac{(-1)^j}{\beta_k} \times \left(\delta_{k1} - \delta_{k2} - 2\pi x_e - 2\pi\lambda \frac{I_0}{\beta_{k+1}} (\delta_{k+1,1} - \delta_{k+1,2} - 2\pi x_e) \right) - \sin(\delta_{kj}) + \eta_{kj}(t) + O(\lambda^2), \quad (25)$$

where $k=1,\ldots,N$, η_{kj} are Gaussian white noise functions of zero mean, $\langle \eta_{kj}(t) \rangle = 0$, and uncorrelated, $\langle \eta_{mi}(t)\eta_{nj}(t') \rangle = 2D\delta_{ij}\delta_{mn}(t-t')$. Since we will be comparing the power spectrum density (PSD) response of a single SQUID ($N=1$) with that of multiple coupled SQUIDs, we set the parameters so that all the SQUIDs are in their running states, absent the coupling; the response at the fundamental of the running frequency will concern us in this section. Figure 8 shows the PSD profile for different ring sizes and for various values of noise intensity. Observe that in each individual panel, where noise intensity is constant, the noise floor in the PSD response curves decreases almost uniformly as the number of SQUIDs in the ring increases. Also, the PSD distribution around the fundamental (of the running frequency) gets more narrowed with increasing *N*. In other words, the frequency response of the ring system becomes more concentrated or well-defined as *N* increases. For any fixed value of *N*, however, the PSD response decreases as noise intensity increases. Another important feature, worth noticing, of the effects of noise is the shift in the fundamental frequency output of the ring. Careful examination shows that, indeed, the frequency output decreases as noise intensity increases. We have observed a similar phenomenon in coupled-core fluxgate magnetometers, except that in this latter system the frequency of a ring of flux gates (unidirectionally coupled) increased as noise intensity increased.

To better understand the relation between the PSD response curves and the noise floor therein, we calculate the signal-to-noise ratio (SNR) (at the fundamental frequency) of an *N*-SQUID ring system in response to changes in coupling strength λ and to the number of SQUIDs *N*, as follows. First, we collect an ensemble of one hundred signals, containing the average output of an *N*-SQUID ring system subject to additive white Gaussian noise, by numerically integrating Eq. (25) with a random set of initial conditions. Then we average the PSD response of the entire ensemble and compute the ratio between the averaged PSD spectrum and the average noise floor measured around the fundamental frequency given by Eq. (24). This ratio yields the SNR surface function shown in Fig. 9. The SNR response for a single SQUID can also be inferred from the values of the surface plot at $\lambda=0$. The plot shows an overall tendency for the SNR output of the coupled ring to increase with small coupling strength. More importantly, the increase, which occurs across different ring sizes, clearly indicates that just a small amount of coupling can significantly strengthen the signal output, relative to background noise, of a ring device; outperforming the output of a single device, in some cases even by a factor of 100%.

The increase in the SNR output seen in Fig. 9 does not extend indefinitely. For a larger range of coupling strength values, the SNR output actually decreases after reaching a peak. The overall profile of the SNR surface resembles what was typically seen in the stochastic resonance cases where

the noise strength is the varying parameter. More importantly, the SNR plot shows that there is an optimal coupling strength which produces the greatest SNR. In addition, a critical observation is the realization that increasing the coupling strength in the ring does not necessarily translate in an increase in its SNR signal output. In fact, it appears that the coupling scheme, rather than the coupling strength, dictates the enhancements in signal output. Consequently, operating the ring device in a weak-coupling regime would suffice to exploit the benefits of the ring configuration. Thus careful tuning of the coupling strength could mitigate the negative effects of noise, and at the same time, such tuning could further enhance the sensitivity of a device underpinned by such a coupled array. Some of these observations had already been made in our earlier (far simpler) analysis of the response of globally coupled dc SQUID rings [31].

IV. THE CASE OF BIDIRECTIONAL COUPLING

In this section we investigate the dynamics of an array of N dc SQUID rings, coupled in a similar fashion to the ring of Sec. III, except that now we consider the rings to be bidirectionally coupled. The flux Φ_k in each individual k SQUID is then given by

$$\Phi_k = \Phi_e + L_k I_k + M I_{k+1} + M I_{k-1},$$

where $k=1,\ldots,N, I_{N+1}=I_1$. Substituting Φ_k into Eq. (2) yields the following system of differential equations for the bidirectionally coupled array:

$$\frac{\tau_k}{I_{0k}}\dot{\delta}_{kj} = J_k + (-1)^j \frac{I_k}{I_{0k}} - \sin(\delta_{kj}), \tag{26}$$

$$\beta_k \frac{I_k}{I_{0k}} = \delta_{k1} - \delta_{k2} - 2\pi x_e - 2\pi\lambda(I_{k-1} + k_{k+1}),$$

where $k=1,\ldots,N \bmod N$, $j=1,2$, $\lambda = M/\Phi_0$, and $\beta_k = 2\pi L_k I_{0k}/\Phi_0$. Computer simulations of the ring equations (26) show oscillatory behavior in the flux dynamics similar to that of the unidirectionally coupled ring. The preferred pattern of oscillation is still the synchronized pattern except that the bidirectional coupling scheme appears to have increased the global stability properties of the synchronized oscillations; typical trajectories now approach the in-phase oscillations much more rapidly than in the unidirectionally coupled ring. The two-parameter bifurcation diagram that depicts the basin boundary of existence of oscillatory solutions and of steady states is qualitatively similar to that of the unidirectional case, see Fig. 2. Assuming the same set of parameter values, the only difference in the diagrams is that the onset of oscillations of the bidirectionally coupled ring $(J_c, x_e = 0.5)$ is shifted, horizontally, towards the right. There is also a maximum coupling strength beyond which the oscillations disappear. To derive an analytic expression for that maximum coupling strength, we employ a similar strategy to that of the unidirectional coupling case. First we solve for I_k using an iterative method. The calculations show that the new ring is still governed by Eq. (14), except that now the bidirectional coupling yields a symmetric matrix B,

$$B = 2\pi\lambda \begin{bmatrix} 0 & 1 & 0 & \ldots & 0 & 1 \\ 1 & 0 & 1 & \ldots & 0 & 0 \\ \vdots & & & \ddots & & \vdots \\ 1 & 0 & 0 & \ldots & 1 & 0 \end{bmatrix},$$

which must be used when solving for I_k through $I = C\Delta$, see Eq. (12). A closed form solution for the matrix C is also possible but it is too cumbersome to be written out. Instead, we take advantage of the coupling strength being relatively small and expand C in powers of λ to get

$$C = \begin{bmatrix} \frac{1}{\beta_1} I_0 & -\frac{1}{\beta_1\beta_2} I_0^2 \varepsilon & 0 & \cdots & 0 & -\frac{1}{\beta_1\beta_N} I_0^2 \varepsilon \\ -\frac{1}{\beta_1\beta_2} I_0^2 \varepsilon & \frac{1}{\beta_2} I_0 & -\frac{1}{\beta_2\beta_3} I_0^2 \varepsilon & \cdots & 0 & 0 \\ \vdots & & & \ddots & & \vdots \\ -\frac{1}{\beta_1\beta_N} I_0^2 \varepsilon & 0 & 0 & \cdots & -\frac{1}{\beta_{N-1}\beta_N} I_0^2 \varepsilon & \frac{1}{\beta_N} I_0 \end{bmatrix} + O(\lambda^2).$$

Rescaling time by τ/I_0, the phase dynamics in Eq. (26) can be written as follows:

$$\dot{\delta}_{kj} = J + \frac{(-1)^j}{\beta_k}\left(\delta_{k1} - \delta_{k2} - 2\pi x_e - 2\pi\lambda \frac{I_0}{\beta_{k+1}}(\delta_{k+1,1} - \delta_{k+1,2} - 2\pi x_e) - 2\pi\lambda \frac{I_0}{\beta_{k-1}}(\delta_{k-1,1} - \delta_{k+1,2} - 2\pi x_e)\right) - \sin(\delta_{kj}) + O(\lambda^2), \tag{27}$$

where $k=1,\ldots,N \bmod N$ and $j=1,2$. As in the case of the unidirectionally coupled ring, λ_{max} is independent of the external flux. So we set $x_e=0$ for simplicity. And again, at λ_{max}, the phase dynamics (27) must be at an equilibrium, in which $\dot{\delta}_{k1} = \dot{\delta}_{k2} = 0$, $\delta_{k1} = \delta_{k+1,1}$, and $\delta_{k2} = \delta_{k+1,2}$. Substituting in Eq. (27) and solving for λ we obtain

$$\lambda_{max}^{b} = \frac{\beta}{4\pi}, \tag{28}$$

where the superscript indicates that the ring is bidirectionally coupled. Again, we note that Eq. (28) is valid for any arbitrary ring size N. Another interesting observation is that the maximum coupling strength that yields flux oscillations in a bidirectionally coupled ring is half that of that of the unidirectionally coupled ring.

To calculate the frequency response of the ring system, we focus our attention on the dynamics of the ring near the bifurcation point $J=J_c$ and rewrite Eq. [27] in terms of the difference and sum variables $\delta_k=(\delta_{k1}-\delta_{k2})/2$ and $\Sigma_k=(\delta_{k1}+\delta_{k2})/2$, leading to

$$\dot{\delta}_k = -\frac{1}{\beta_k}(2\delta_k - 2\pi x_e) + 2\pi\lambda\frac{I_0}{\beta_k\beta_{k+1}}(2\delta_{k+1} - 2\pi x_e) + 2\pi\lambda\frac{I_0}{\beta_k\beta_{k-1}}(2\delta_{k-1} - 2\pi x_e) - \cos\Sigma_k \sin\delta_k,$$

$$\dot{\Sigma}_k = J - \cos\delta_k \sin\Sigma_k. \tag{29}$$

Let $(\delta_{k0},\Sigma_{k0})$ denote the fixed point of each individual, uncoupled, SQUID. Also let $x_k=\delta_k-\delta_{k0}$, $y_k=\Sigma_k-\Sigma_{k0}$. A Taylor series of expansion of Eq. (18) about $J-J_c$, up to third order, yields

$$\dot{x}_k = -\left(\frac{2}{\beta_k} + A_k\right)x_k + B_k y_k + \frac{\varepsilon I_0}{\beta_k\beta_{k+1}}(2\delta_{k-1,0} - 2\pi x_e) + \frac{\varepsilon I_0}{\beta_k\beta_{k-1}}(2\delta_{k-1,0} - 2\pi x_e) + \frac{2\varepsilon I_0}{\beta_k\beta_{k+1}}x_{k+1} + \frac{2\varepsilon I_0}{\beta_k\beta_{k-1}}x_{k-1} + C_k x_k^2 + 2D_k x_k y_k + C_k y_k^2,$$

$$\dot{y}_k = (J - J_c) - A_k y_k + B_k x_k + D_k y_k^2 + 2C_k x_k y_k + D_k x_k^2, \tag{30}$$

$$j = 0,$$

$$\dot{\lambda} = 0,$$

where $A_k=\cos\Sigma_{k0}\cos\delta_{k0}$, $B_k=\sin\Sigma_{k0}\sin\delta_{k0}$, $C_k=(1/2)\cos\Sigma_{k0}\sin\delta_{k0}$, and $D_k=(1/2)\sin\Sigma_{k0}\cos\delta_{k0}$. We then determine the frequency of the oscillations in the bidirectionally ring from a reduction of Eq. (30) to its center manifold. The procedure is very similar to the one we employ to find the frequency of oscillations in unidirectionally coupled rings, and we simply summarize the main results. Direct calculations show that the dynamics of Eq. (30) on its center manifold is given by

$$u_1(t) = \sqrt{\frac{F_b}{\alpha} - \frac{\gamma^2\varepsilon^4}{\alpha^2}}\tan(\sqrt{F_b\alpha - \gamma^2\varepsilon^4}t) - \frac{\gamma\varepsilon^2}{\alpha}, \tag{31}$$

where the coefficient F_b is now $F_b=(J-J_c)\cos\theta_1 - [\varepsilon/(\beta_1\beta_2)(2\delta_{20}-2\pi x_e)+\varepsilon/(\beta_1\beta_N)(2\delta_{N0}-2\pi x_e)]\sin\theta_1$. It follows that the frequency of the oscillations of the bidirectionally coupled SQUID ring system (27) is given by

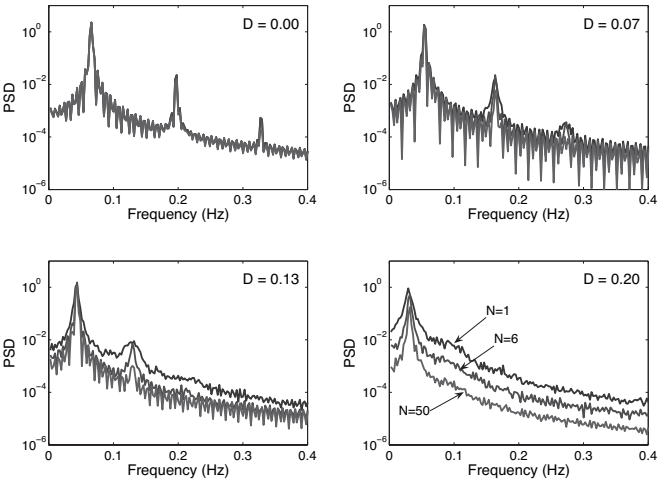

FIG. 10. Average PSD response of a N-SQUID ring system, bidirectionally coupled, to various values of noise amplitude. Parameters are $J=0.5$, $x_e=0.5$, $\beta_k=0.8$, $\lambda=0.01$. Observe that in each individual panel the noise floor decreases as the number of SQUIDs increases. In all three cases, noise floor rises, however, as the noise amplitude increases.

$$\omega_b = \frac{1}{2\pi}\sqrt{F_b\alpha - \gamma^2\varepsilon^4}. \tag{32}$$

Observe that the dynamics on the center manifold depends now on the phase dynamics of two neighboring SQUIDs, instead of just one. This result is expected since the SQUIDs are now bidirectionally coupled. Consequently, the frequency response of both, unidirectionally and bidirectionally coupled rings, is independent of the number of SQUIDs. On the contrary, the mean-field coupling in the all-to-all network configuration of Acebron *et al.* [6] leads to a frequency dependence on the number of SQUIDs. Nevertheless, the frequency output of all these three different networks scales as a square-root of the coupling strength.

Figure 10 now illustrates the power spectrum decomposition of the oscillatory signal output of a bidirectionally coupled SQUID ring system. The spectral response appears to be of the same order as in the unidirectionally coupled rings, see Fig. 8, including the shift in the fundamental frequency ouput. But careful examination shows that the noise floor in the unidirectional case tends to decrease, with increasing N, more so than in the bidirectionally coupled ring.

To investigate further the effects of noise, we have also calculated the SNR output (see Fig. 11), at the fundamental of the oscillation frequency. The magnitude and profile of the SNR output are comparable to those of the unidirectional ring. That is, the SNR output of the bidirectionally coupled ring also increases with weak coupling until reaching a peak value at an optimal coupling strength and decreases for stronger coupling strengths. For both the unidirectionally coupled and the bidirectionally coupled systems, the SNR surfaces in Figs. 9 and 11 show a certain rippling feature along the up slope and the down slope of the SNR profile. These features are not artifacts from the numerics. Instead, we believe they are the inherent result of the dynamics of the coupled systems. We do not attempt to investigate the source of these ripple effects in this work.

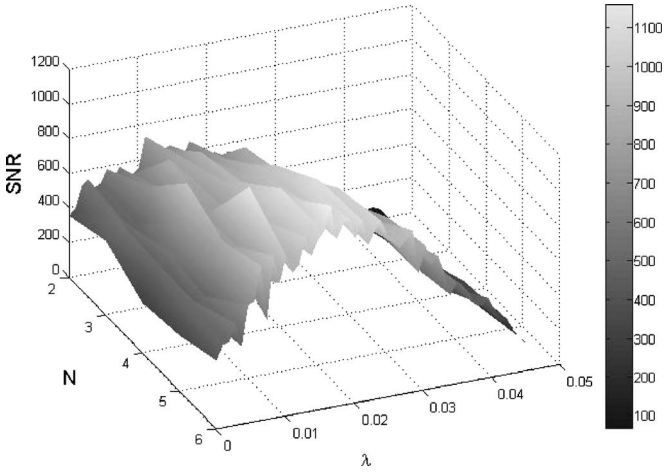

FIG. 11. Average signal-to-noise-ratio response of a N-SQUID, bidirectionally coupled, ring system as a multifunction of coupling strength λ and of the number of SQUIDs N, starting with $N=3$. Parameters are $J=0.5$, $x_e=0.5$, $\beta_k=0.8$, $D=0.5$.

V. DISCUSSION AND CONCLUSIONS

We have investigated the dynamics of two rings of locally coupled SQUID sensors, one unidirectionally coupled and one bidirectionally coupled, and have compared their response characteristics to those of a ring with all-to-all mean-field coupling. A two-parameter bifurcation analysis reveals that all of these rings exhibit similar regions of existence of steady-state solutions and of coupling-induced oscillations. Within the running solution regime, the preferred pattern of oscillation is a completely synchronized pattern in which flux oscillations among the SQUIDs are in phase with one another and the amplitude of the oscillations is also the same. In all three rings, the frequency response shows a dependence on the coupling strength that follows a square-root scaling law. In the locally coupled rings, however, the frequency output is independent of the number of SQUIDs in the ring. In the all-to-all coupled ring, on the contrary, the mean-field coupling scheme yields a frequency response [6] that depends on the size of the ring; in addition, the mean-field description is not expected to hold for small N, in contrast to the results of this work. Both rings, unidirectionally coupled and bidirectionally coupled, show comparable improvements in signal output, relative to background noise, over those of a single device. A critical observation is the realization that a local coupling scheme can significantly enhance the sensitivity of a ring-based device, and the improvements can be achieved even with weak coupling strength.

We now give a perspective for a potential experimental realization of the SQUID-ring systems considered in this work. We first observe that the coupling scheme described by Eqs. (11) acts locally, inductively coupling (unidirectionally) the circulating current of one SQUID to its nearest neighbor. Unlike the globally coupled SQUID system studied by Acebron *et al.* [6], where the system has a large number of inputs resulting from the globally coupling terms, here the number of inputs is one and at most two for the unidirectionally coupled system and the bidirectionally coupled system, respectively. This small number of inputs to each element makes the system simpler to implement in experiments. The experimental realization of a dc-SQUID ring system can be accomplished by measuring the circulating current of a nearest neighbor's element and couple that current (after some appropriate signal conditioning) to the present SQUID.

We note also that, although the coupling scheme is based on previous work on coupled-core fluxgate magnetometers, it is important to clarify and emphasize that the resulting coupled-SQUID device would be significantly different for the following reasons. A single-core fluxgate magnetometer does not produce oscillatory behavior unless a bias signal (of amplitude sufficient to drive the ferromagnetic core between its stable steady states) is applied. A single dc SQUID can oscillate by itself, however, if it is properly tuned past the critical onset point J_c. Consequently, the dynamics of the coupled-SQUID system are significantly different, in fact, far richer than those of a coupled-core fluxgate magnetometer.

We note, in closing, that the results (and procedures) of this work should be applicable to networks of other excitable systems that pass through bifurcations to oscillatory solutions; one example is the well-known Fitzhugh-Nagummo model of excitable cells for which a globally coupled mean-field treatment (for a large N network) has already been carried out [36].

ACKNOWLEDGMENTS

The authors acknowledge support from the Office of Naval Research (Code 331). P.L. and A.P. were supported in part by U.S. Space and Naval Warfare Systems Command Grant No. N66001-06-M-108.

[1] M. Inchiosa, A. Bulsara, K. Wiesenfeld, and L. Gammaitoni, Phys. Lett. A **252**, 20 (1999).
[2] M. Inchiosa, V. In, A. Bulsara, K. Wiesenfeld, T. Heath, and M. Choi, Phys. Rev. E **63**, 066114 (2001).
[3] A. Bulsara, V. In, A. Kho, P. Longhini, A. Palacios, W. Rappel, J. Acebron, S. Baglio, and B. Ando, Phys. Rev. E **70**, 036103 (2004).
[4] V. In, V. Sacco, A. Kho, S. Baglio, B. Ando, A. Bulsara, and A. Palacios, IEEE Sens. J. (to be published).
[5] See, e.g., A. Barone and G. Paterno, *Physics and Applications of the Josephson Effect* (Wiley, New York, 1982); *The SQUID Handbook*, edited by J. Clarke and A. I. Braginski (Wiley-VCH, New York, 2004), Vol. 1; J. Clarke, in *The New Superconducting Electronics*, edited by H. Weinstock and R. Ralston (Kluwer, Amsterdam, 1993), pp. 123–180; D. Koelle, R. Kleiner, F. Ludwig, E. Dankster, and J. Clarke, Rev. Mod. Phys. **71**, 631 (1999).
[6] J. Acebron, A. Bulsara, M. Inchiosa, and W.-J. Rappel, Euro-

phys. Lett. **56**, 354 (2001); J. Acebron, W. Rappel, and A. Bulsara, Phys. Rev. E **67**, 016210 (2003); Fluct. Noise Lett. **3**, L341 (2003).
[7] D. Cohen, Science **175**, 664 (1972).
[8] G. B. Donaldson, in *Superconducting Electronics*, edited by H. Weinstock and M. Nisenoff (Springer-Verlag, New York, 1980), pp. 175–207.
[9] P. Hadley and M. R. Beasley, Appl. Phys. Lett. **50**, 621 (1987).
[10] R. L. Fagaly, IEEE Trans. Magn. **25**, 1204 (1989).
[11] H. Weinstock, IEEE Trans. Magn. **27**, 3231 (1991).
[12] A. D. Hibbs, R. E. Sager, D. W. Cox, T. H. Aukerman, T. A. Sage, and R. S. Landis, Rev. Sci. Instrum. **63**, 3652 (1992).
[13] S. Tan, Y. P. Ma, I. M. Thomas, and J. P. Wikswo, IEEE Trans. Appl. Supercond. **3**, 1945 (1993).
[14] M. Radparvar and S. Rylov, IEEE Trans. Appl. Supercond. **5**, 2142 (1995).
[15] O. V. Lounasmaa, Phys. Scr. **T66**, 70 (1996).
[16] G. L. Romani, C. Del Gratta, and V. Pizzella, in *SQUID Sensors: Fundamentals, Fabrication and Applications*, edited by H. Weinstock (Kluwer Academic Publishers, Amsterdam, 1996), pp. 445–490.
[17] J. P. Wikswo, *SQUID Sensors: Fundamentals, Fabrication and Applications* (Ref. [16]), pp. 307–360.
[18] J. P. Wikswo, in *Applications of Superconductivity*, edited by H. Weinstock (Kluwer Academic Publishers, Amsterdam 2000), pp. 139–228.
[19] H. Yabuki, *Quasi-Planar SNS Junction as a Sensor for Brain Studies, Riken-The Institute of Physical and Chemical Research*, www.riken.go.jp/Yoran/BSIS/140B-141.html
[20] J. Oppenlander, Ch. Haussler, and N. Schopohl, Phys. Rev. B **63**, 024511 (2001); J. Oppenlaender, T. Traeuble, Ch. Haeussler, and N. Schopohl, IEEE Trans. Appl. Supercond. **11**, 1271 (2000); V. Schultze, R. Jesselsteijn, H.-G. Meyer, J. Oppenlaender, Ch. Haeussler, and N. Schopohl, *ibid.* **13**, 775 (2003); J. Oppenlaender, P. Caputo, Ch. Haeussler, T. Traeuble, J. Tomes, A. Friesch, and N. Schopohl, Appl. Phys. Lett. **83**, 969 (2003).
[21] A. Hibbs and B. Whitecotton, in *Applied Nonlinear Dynamics and Stochastic Systems Near the Millenium*, edited by J. Kadtke and A. Bulsara (AIP, Woodbury, NY, 1997); M. Inchiosa, A. Bulsara, A. Hibbs, and B. Whitecotton, Phys. Rev. Lett. **80**, 1381 (1998); M. Inchiosa, A. Bulsara, K. Wiesenfeld, and L. Gammaitoni, Phys. Lett. A **252**, 20 (1999).
[22] J. Z. Sun, W. J. Gallagher, and R. H. Koch, Appl. Phys. Lett. **61**, 3190 (1992).
[23] A. de Waele and R. de Bruyn Ouboter, Physica (Amsterdam) **41**, 225 (1969); A. Matsinger, R. de Bruyn Ouboter, and H. van Beelen, Physica B & C **94B**, 91 (1978); C. Tesche, J. Low Temp. Phys. **44**, 119 (1981); E. Ben-Jacob, D. Bergman, Y. Imry, B. Matkowsky, and Z. Schuss, J. Appl. Phys. **54**, 6533 (1983); T. Ryhanen, H. Seppa, R. Ilmoniemi, and J. Knuutila, J. Low Temp. Phys. **76**, 287 (1989).
[24] See, e.g., N. Minorsky, *Nonlinear Oscillations* (Kreiger, New York, 1987).
[25] K. Wiesenfeld, A. Bulsara, and M. Inchiosa, Phys. Rev. B **62**, R9232 (2000).
[26] A. Mikhailov and Y. Loskutov, *Foundations of Synergetics* (Springer Verlag, Berlin, 1996), Vols. 1, 2; J. Garcia-Ojalvo and J. Sancho, *Noise in Spatially Extended Systems* (Springer-Verlag, Berlin, 1999); M. Locher, *Noise Sustained Patterns* (World Scientific, Singapore, 2002).
[27] A. Sarmiento, R. Reigada, A. Romero, and K. Lindenberg, Phys. Rev. E **60**, 5317 (1999); R. Regeida, A. Sarmiento, A. Romero, J. Sancho, and K. Lindenberg, J. Chem. Phys. **112**, 10615 (2000); R. Reigada, A. Sarmiento, and K. Lindenberg, Phys. Rev. E **63**, 066113 (2001); R. Regeida, A. Sarmiento, and K. Lindenberg, Physica A **305**, 467 (2002); H. Wio and K. Lindenberg, in *Modern Challenges in Statistical Mechanics: Patterns, Noise, and the Interplay of Nonlinearity and Complexity*, AIP Conf. Proc. No. 658, edited by V. Kenkre and K. Lindenberg (AIP, Melville, NY, 2003).
[28] M. Shiino, Phys. Rev. A **36**, 2393 (1987).
[29] See, e.g., A. Pikovsky, M. Rosenblum, and J. Kurths, *Synchronization: A Universal Concept in Nonlinear Sciences* (Cambridge University Press, Cambridge, England,2003); J. Acebron, L. Bonilla, C. Perez Vicente, F. Ritort, and R. Spigler, Rev. Mod. Phys. **77**, 137 (2005).
[30] See, e.g., M. Locher, D. Cigna, E. Hunt, G. Johnson, F. Marchesoni, L. Gammaitoni, M. Inchiosa, and A. Bulsara, Chaos **8**, 604 (1998), and references therein.
[31] M. Inchiosa and A. Bulsara, in *Stochastic and Chaotic Dynamics in the Lakes*, edited by D. S. Broomhead, E. Luchinskaya, P. V. E. McClintock, and T. Mullin (AIP, Melville, NY, 2000).
[32] V. In, A. Bulsara, A. Palacios, P. Longhini, and A. Kho, Phys. Rev. E **72**, 045104(R) (2005).
[33] V. In, A. Palacios, A. Bulsara, P. Longhini, A. Kho, J. Neff, S. Baglio, and B. Ando, Phys. Rev. E **73**, 066121 (2006).
[34] A. Bulsara, J. Lindner, V. In, A. Kho, S. Baglio, V. Sacco, B. Ando, P. Longhini, A. Palacios, and W.-J. Rappel, Phys. Lett. A **353**, 4 (2006).
[35] J. Lindner and A. Bulsara, Phys. Rev. E. (to be published).
[36] J. Acebron, A. Bulsara, and W.-J. Rappel, Phys. Rev. E **69**, 026202 (2004); *Proceedings of the IUTAM Meeting on Nonlinear Stochastic Dynamics, Urbana, Illinois 2002*.